Hydrogen Induced Rupture of Si–O Bonds in Amorphous Silicon Dioxide

Al-Moatasem El-Sayed,[1,*] Matthew B. Watkins,[1,†] Tibor Grasser,[2,‡] Valery V. Afanas'ev,[3,§] and Alexander L. Shluger[1,¶]

[1] *Department of Physics and Astronomy and London Centre for Nanotechnology, University College London, Gower Street, London, WC1E 6BT, United Kingdom*
[2] *Institute for Microelectronics, Technische Universität Wien, A-1040, Vienna, Austria*
[3] *Department of Physics, University of Leuven, Celestijnenlaan 200D, 3001 Leuven, Belgium*

(Dated: October 23, 2014)

Using *ab initio* modeling we demonstrate that H atoms can break strained Si–O bonds in continuous amorphous (a)-SiO_2 networks, resulting in a defect consisting of a 3-coordinated Si atom with an unpaired electron facing a hydroxyl group, adding to the density of dangling bond defects, such as E′ centres. The barriers to form this defect from interstitial H atoms range between 0.5 and 1.3 eV. This discovery of unexpected reactivity of atomic hydrogen may have significant implications for our understanding of processes in nano-scaled silica, e.g., in porous low-permittivity insulators, and strained variants of a-SiO_2.

The interaction of hydrogen with wide band gap oxides and minerals is important for many applications and has been a subject of a number of experimental and theoretical studies (see refs. [1–7] to mention a few). Among these, quartz and amorphous (a)-SiO_2 occupy a very prominent role due to their abundance and fundamental and technological importance. Examples of hydrogen and water induced effects include hydrolytic weakening of quartz and minerals [8], degradation phenomena in optical fibers [9] and in SiO_2-insulated electronic devices, such as radiation damage [10–12], as well as injection-induced [13] and bias-temperature instabilities [14, 15]. Hydrogen usually passivates dangling Si and Si–O bonds in silica as revealed by infrared spectroscopy [16, 17]. However, the role of atomic hydrogen in silica degradation processes is still poorly understood.

In the silica glass community, synthetic wet samples containing high concentrations of bound hydroxyl (Si–O–H) groups are widely used for UV optics. The presence of Si–O–H groups is shown to improve the near UV transparency of this type of glass by reducing the concentrations of oxygen deficiency-related defects and strained Si–O bonds. Radiolysis [18, 19] and photolysis of wet silica glass – e.g. using ArF and F_2 lasers [4, 16, 17] – readily creates high concentrations of atomic hydrogen. Hydrogen atoms rapidly diffuse through the silica network with activation energies of about 0.2 eV [4, 5] and interact with other defects, such as Si dangling bonds and passivated Si–H bonds, forming several H-related paramagnetic centers. These centers have been characterized by electron paramagnetic resonance (EPR). In particular, a 7.4 mT doublet in the EPR spectra has been assigned to a Si dangling bond coordinated by two bridging oxygens and a hydrogen atom and is known as the H(I)-center [20, 21]. A 1.05 mT doublet in the EPR spectra of irradiated silica glass is shown to be due to the forbidden nuclear spin-flip transitions of a proton, made possible by a weak hyperfine interaction with the unpaired electron of a nascent Si dangling bond, so called E′-center [17]. This defect does not exhibit a detectable hyperfine splitting on a proton which is thought to be due to the fast proton motion. A 0.08 mT doublet due to proton hyperfine splitting has been assigned to a Si dangling bond coordinated by two bridging oxygens and an OH group (so called E′(OH)-center) [16]. This defect is thought to result from a reaction of H^0 with electronically excited strained Si–O bonds [16]. However, detailed mechanisms for creation of these defects are still unknown.

On the other hand, analysis of defects in the most chemically pure a-SiO_2 layers grown by thermal oxidation of silicon and, therefore, not compromised by the presence of other impurities, has also shown that a supply of hydrogen during thermal treatment or illumination may lead to formation of additional densities of intrinsic network defects [15]. Critically, they exceed the density of the same defects in identical a-SiO_2 films processed in the absence of hydrogen [22]. These additional defects are also predominantly Si dangling bonds in SiO_2 (E′-type centres: $O_3 \equiv Si^{\bullet}$ entity, where the dot symbolises an unpaired electron [23]) or at the Si/SiO_2 interface (P_b-type centres: $Si_3 \equiv Si^{\bullet}$ entity [24, 25]), suggesting that H-induced bond rupture occurs in the ostensibly defect-free a-SiO_2 network and at the Si/a-SiO_2 interface. Accumulation of hydrogen inside the a-SiO_2 film revealed by a variety of methods firmly supports this conjecture and further suggests that the broken bonds are passivated by hydrogen. [26, 27] Remarkably, hydrogen enhances the mobility of O atoms, which can be even removed from the a-SiO_2 layer to silicon substrate. [28, 29] Although the Si–O bond rupture was initially correlated with the presence of protonic species [30, 31] formed by hole trapping [32] or hydrogen ionisation at the Si/SiO_2 interface, [33] the involvement of H^0 should also be considered since it is far more abundant than radiolytic protons.

Theoretically, Edwards and Germann used semi-emprirical calculations in cluster models to study several hydrogen related defects in silica and observed the insertion of H^0 into a strained Si–O bond [34]. Pacchioni and

Vitiello used the Hartree-Fock method and small clusters to calculate the IR and EPR parameters of several H related defects in silica [35]. Periodic Density Functional Theory (DFT) calculations suggested that H^0 interacts weakly with perfect crystalline α-quartz and amorphous silica [7, 36].

To summarize our current perception of atomic hydrogen's interaction with a-SiO_2: it passivates defective sites, otherwise interacting negligibly with the a-SiO_2 network. Here we use atomistic simulations and ab intio calculations to demonstrate that, contrary to common perceptions, atomic hydrogen can break strained Si–O bonds in defect-free a-SiO_2 networks, generating a three-coordinated Si dangling bond facing a hydroxyl O–H group [see Fig. 1b]. The critical factor which makes creation of this defect feasible is the disorder of the a-SiO_2 matrix which results in the presence of strained Si–O bonds. Structural disorder makes the revealed mechanism pertinent to defect generation in complex silicate glasses, natural minerals, and tectosilicate materials in general.

To build up a distribution of defect properties, the ReaxFF [37, 38] force-field was used to generate 116 periodic models of a-SiO_2, each containing 216 atoms. All classical atomistic simulations were performed using the LAMMPS code. [39] To generate the amorphous structures, classical molecular dynamics simulations were run to melt and quench crystalline SiO_2 structures into an amorphous state, as described in detail in ref.[40]. Densities of the ReaxFF a-SiO_2 structures range from 2.05 to 2.20 g cm^{-3}, averaging at 2.13 g cm^{-3} in agreement with the range of densities known for a-SiO_2. [41]

Density functional theory (DFT), implemented in the CP2K code [42], was used to further optimise the geometries of amorphous structures and calculate their electronic structures. The non-local functional PBE0_TC_LRC was used in all calculations with a cutoff radius of 2.0 Å. [43] Inclusion of Hartree-Fock exchange provides an accurate description of the band gap and localised states that may be involved in charge trapping processes. The CP2K code uses a Gaussian basis set with an auxiliary plane-wave basis set. [44] We employed a double-ζ basis set with polarization functions [45] for all atoms in conjunction with the Goedecker-Teter-Hutter (GTH) pseudopotential. [46] Calculating hyperfine interactions necessitated the use of all electron basis sets using the Gaussian and augmented plane-wave (GAPW) approach. The basis sets with contraction schemes of (8831/831/1),(8411/411/11) and 6-311G** were used for silicon [47], oxygen [48] and H, [49] respectively. The plane wave cut-off was set to 5440 eV (400 Ry). To reduce the computational cost of non-local functional calculations, the auxiliary density matrix method (ADMM) was employed. [50] The density is mapped onto a much sparser Gaussian basis set containing less diffuse and fewer primitive Gaussian functions than the one employed in the rest of the calculation.

All geometry optimizations were performed using the BFGS optimiser to minimise forces on atoms to within 37 pN (2.3 $\times 10^{-2}$ eV Å^{-1}). Cell vectors were not allowed to relax. Barriers between configurations were calculated using the climbing image nudged elastic band method (CI-NEB). [51] Linear interpolation was used to generate 10 images to be optimised, with each of the images connected by a spring with a force constant of 2 eV Å^2.

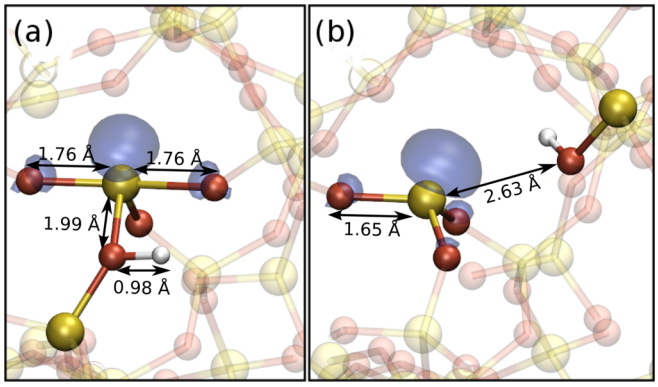

FIG. 1. Atomic configuration and spin density of two hydrogen induced defects. The Si atoms are the bigger yellow balls, the O atoms are the smaller red balls and the H atom is the small white ball in each configuration. The spin densities are the blue, transparent polyhedra. a) The $[SiO_4/H]^0$ centre where the Si–O bond is still intact and the spin density is localised on the central Si atom and two of its O neighbors. A proton is attached to the bridging O at the bottom of the configuration. b) The hydroxyl E′ centre where the spin density is localised on the Si and its three O neighbors. The 3-coordinated Si faces a hydroxyl group.

Following suggestions by previous studies, we first placed a single H atom in random positions in a-SiO_2 samples under the constraint that it is further than 2 Å from its nearest neighbor. [36, 52] Minimizing the total energy of 26 independent samples with respect to the atomic coordinates shows that in these positions the interstitial H atom only weakly interacts with the a-SiO_2 network, with the nearest neighbors found at $\approx$ 2.6 Å. The spin density is almost entirely localised on the H atom and a one-electron level is located in the a-SiO_2 band-gap at 0.7 eV above the valence band, in accord with previous studies. [52] Similarly, the H_2 molecule prefers locations in the middle of voids in a-SiO_2 structure and interacts negligibly with the matrix, again in good agreement with the previous calculations. [36, 53]

We note that the interstitial configuration of H atom is similar to that of Li atom in α-quartz. However, as shown in ref. [40], a more stable configuration of the so-called $[SiO_4/Li]^0$ centre corresponds to the electron transfer from an interstitial Li atom to a network Si ion accompanied by the opening of a O–Si–O angle to 150°. To investigate whether H atoms can form similar binding

configurations in a-SiO_2, they were placed randomly at a distance of ≈ 1 Å from O atoms in 116 different non-defective samples. The geometry optimizations resulted in two new types of H–related defect centers.

In the first type, H is bound to a bridging O atom with a bond length of 0.97 Å on average. This is accompanied by the opening of an O–Si–O angle of one of the Si neighbors of the bridging O and an electron transfer from the H atom onto this Si neighbor. This creates the configuration shown in Fig. 1a whereby a proton is bound to the bridging oxygen with an unpaired electron localised on a four-coordinated Si atom. This configuration is indeed similar to the $[SiO_4/Li]^0$ centre and to an electron trap configuration in a-SiO_2 matrix discussed in recent papers. [40, 54] Therefore, we will call it a $[SiO_4/H]^0$ centre. The manner in which the proton binds to the bridging O is similar to the protonic interactions in SiO_2 described in the literature. [36, 53, 55–57] The barrier to forming this configuration from an interstitial H atom is about 1.8 eV whereas its total energy is very similar to that of the interstitial H atom. Indeed, the difference in total energies in different samples ranges from 0.2 eV more stable to 0.1 eV less stable than the interstitial H configuration. This defect introduces a one-electron state in the band gap at about 3.5 eV above the a-SiO_2 valence band with mainly Si 'sp' character with a contribution from O 'p' orbitals.

The Si atom on which the electron is localised is the one associated with the longer Si–O bond around the bridging O. The O–Si–O angle of the Si ion with a trapped electron extends to an average of 165°, ranging from 162° to 170°, with the two Si–O bonds associated with this angle extending to an average of 1.76 Å, ranging from 1.72 Å to 1.88 Å. The Si–O bond where the H binds to the bridging O extends to an average of 1.99 Å (see Fig. 1a), significantly weakening this Si–O bond, while the remaining Si–O bond in the SiO_4 tetrahedron stays at 1.64 Å.

The results [34]predict that H^0 can be trapped at SiO_2 network sites under moderate tensile strain. Further analysis of the different defect configurations explored in our simulations showed that placing an H atom 1.0 Å away from O atoms associated with strained Si–O bonds longer than 1.65 Å in 116 different defect-free a-SiO_2 samples creates the second type of defect centre, where the H atom breaks an Si–O bond and a hydroxyl group is formed in its place [see Fig. 1b]. The Si facing the hydroxyl group is now 3-coordinated with an unpaired electron residing on it. The unpaired spin is strongly localised on the Si atom with the average Mulliken spin moment of the 3-coordinated Si equal 0.90, ranging from 0.84 to 0.98. The calculated average values of hyperfine splitting on Si, the nearest neighbor O ions and H of the O–H group are 48.4 mT, 3.0 mT and 0.1 mT, respectively. This configuration resembles an E′ centre perturbed by a nascent OH group, and so it shall be referred to as a

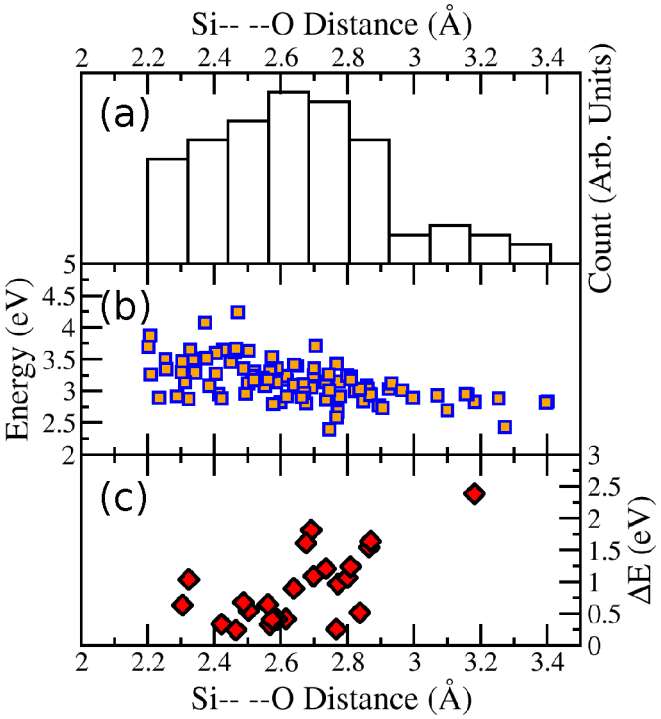

FIG. 2. Correlations between the one-electron levels and relative stabilities of the hydroxyl E′ centre with the non-bonding Si– –O interaction. (a) A histogram of the distribution of the Si– –O distances in the hydroxyl E′ defect structure [see Fig. 1b]; (b) energies of the one-electron defect levels with respect to the top of the a-SiO_2 valence band plotted against the Si– –O distance; (c) the relative stability of the hydroxyl E′ with respect to an interstitial H atom, plotted against the Si– –O distance.

hydroxyl E′ centre to distinguish from the E′(OH)-center proposed in [16]. Although both centers have very similar hyperfine splittings on H atom, our calculations demonstrate a wide spread of H hyperfine values (0.05–0.15 mT) and do not involve excitation of Si–O bonds.

The hydroxyl E′ centre is by far more thermodynamically stable than the $[SiO_4/H]^0$ centre and is lower in energy by 0.8 eV on average than the interstitial H atom in the SiO_2 network (the relative stability, ΔE, ranges from a minimum of 0.3 eV to a maximum of 2.3 eV lower than the energy of interstitial H atom, see Figure 2(c)). Further calculations also show that the barrier for conversion from a $[SiO_4/H]^0$ centre into a hydroxyl E′ centre is less than 0.1 eV. However, the barrier for an interstitial H atom to break a Si–O bond and form this centre calculated from 13 different models averages at 1.0 eV, ranging between 0.5 eV and 1.3 eV.

The Si–O bonds of the $O_3 \equiv Si^{\bullet}$ moiety in the hydroxyl E′ centre average at 1.65 Å (from the 116 independent configurations considered) while the distance between the dissociated Si and O atoms [see Fig. 1b] average at 2.63 Å exhibiting a wide distribution, shown in Figure 2(a). This figure also demonstrates the position of the one-

Reaction	Forward Reactions			Reverse Reactions			ΔE
	Min.	Max.	Avg.	Min.	Max.	Avg.	
1) $O_3 \equiv Si\overset{O}{\diagup\diagdown}Si \equiv O_3 + H^0 \rightleftharpoons O_3 \equiv Si\cdot\overset{HO}{\diagdown}Si \equiv O_3$	0.50	1.71	0.91	1.25	2.40	1.66	-0.75
2) 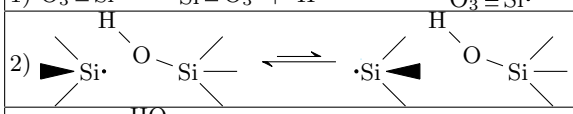	1.00	2.34	1.75	0.31	1.89	1.08	0.67
3) $O_3 \equiv Si\cdot\overset{HO}{\diagdown}Si \equiv O_3 + H^0 \rightleftharpoons O_3 \equiv Si - H\overset{HO}{\diagdown}Si \equiv O_3$	0.00	0.00	0.00	3.96	4.31	4.19	-4.19
4) $O_3 \equiv Si\overset{O}{\diagup\diagdown}Si \equiv O_3 + H_2 \rightleftharpoons O_3 \equiv Si - H\overset{HO}{\diagdown}Si \equiv O_3$	1.07	2.15	1.74	1.57	2.45	1.94	-0.20

TABLE I. The calculated reaction barriers and relative energies (in eV) of hydrogen interaction with the a-SiO_2 matrix. ΔE is the total energy difference between the left and right hand sides of each reaction. 1) H atom attacking a bridging O to produce the hydroxyl E′ centre. 2) Relaxation of Si dangling bond through the plane of its neighbors to form the back-projected configuration. 3) Atomic H passivating the hydroxyl E′ centre. 4) H_2 molecule attacking a bridging O to make the passivated configuration of the hydroxyl E′ centre. Longer arrow corresponds to lower reaction barriers.

electron defect level with respect to the top of the valence band correlates with the non-bonding Si– –O distance. The average position of the one-electron level is about 3.1 eV above the a-SiO_2 valence band. The further away Si and the negative O ion are from each other, the deeper (closer to the top of the valence band) the defect level becomes as this reduces the repulsion between the unpaired electron and O ion. This reduction in repulsion energy also increases the relative stability of the hydroxyl E′ centre with respect to H interstitial atom, as seen in 2 (c).

Interstitial H^0 in perfect wide gap crystalline oxides, including α-quartz, behaves as a negative U center; it is thermodynamically unstable in the neutral charge state, preferring to convert into H^+ or H^- depending on the position of the Fermi level [1–4, 6, 7]. In a separate paper, [58] we demonstrate that some hydroxyl E′ centres retain the negative U behaviour, however, a significant part of the neutral hydroxyl E′ centres in our sample prove to be the most thermodynamically stable hydrogenic state across the whole a-SiO_2 band gap.

The hydroxyl E′ centre can take part in several further reactions involving hydrogen atoms and molecules, as summarised in Table I. Reaction 2 corresponds to the formation of a second, so called back-projected, isomer of the hydroxyl E′ centre. In this reaction, the Si dangling bond moves through the plane of its three O neighbors forming a stable state where the Si is inverted with respect to the original configuration. This requires overcoming a significant energy barrier of 1.8 eV [see reaction 2 in table I], but creates a defect configuration with an unpaired electron now facing away from the Si–O–H group. The local geometry of this back-projected configuration is rather similar to the original configuration, but the distance between the 3-coordinated Si and the hydroxyl group increases to an average of 3.43 Å. We find that the original configuration is on average 0.7 eV more stable than this back-projected configuration.

Reaction 3 corresponds to the barrier-less passivation of the hydroxyl E′ centre by atomic hydrogen. The calculated binding energy of the Si–H bond that is formed after passivation averages at 4.2 eV from 13 systems, ranging from 4.0 eV to 4.3 eV. The length of Si–H bonds in a-SiO_2 has a very narrow distribution in contrast to those associated with the Si and O atoms, in agreement with the common perception that the Si–H bond is very stable and hence the passivation is very effective. The barrier for the de-passivation, the reverse of reaction 3, in this case, is about 4.2 eV, i.e. the strength of the Si–H bond. Passivation of the hydroxyl E′ centre eliminates the defect levels in the a-SiO_2 band gap.

We note that the same passivated defect state can be created via dissociation of an H_2 molecule at a strained Si–O bond in the a-SiO_2 network (reaction 4 in table I). Although the passivated state is on average more stable than an interstitial H_2 molecule, the barriers for both the forwards and reverse reactions are much higher because they either require breaking a strong H–H bond (forward), or breaking strong Si–H and O–H bonds (reverse). These results suggest that the concentration of hydroxyl E′ centres strongly depends on the sample history and the concentration of molecular and atomic hydrogen.

To summarise, our results clearly demonstrate that the presence of strained bonds in a-SiO_2 gives rise to an additional channel of interaction of H atoms with a-SiO_2 networks, predicting the formation of a hydroxyl E′ centre. Hence H^0 is not always a benign agent in defect-free SiO_2 network and can produce thermodynamically stable neutral defects in a-SiO_2, adding to the density of dangling bond defects, such as E′ centres.

We note that extreme bondings in the oxide are expected to become more abundant under influence of strain and hence this discovery of unexpected reactivity of atomic hydrogen may have significant implications for our understanding of processes in nano-scaled silica,

e.g., in porous low-permittivity insulators, and strained variants of a-SiO_2. It may also shed a new light on the behavior of atomic hydrogen in other amorphous solids as well as on the so-called hydrogen spillover. [59]. For example, it has recently been reported by many researchers that application of catalytic metal electrodes such as Pt [60], Pd [61], or Ru [62], in combination with annealing in H-containing ambient allows one to improve the electrical properties of a wide range of device structures. This observation points towards the effect(s) of atomic H production and its interaction; since the reversible behavior expected for the classical passivation-depassivation scheme is not reported, the most plausible explanation is the interaction of hydrogen with amorphous interlayers or grain boundaries in a way similar to the mechanism described here

The authors acknowledge EPSRC and the EU FP7 project MORDRED (EU Project grant No. 261868) and COST Action CM1104 for financial support. We would like to thank the UK's HPC Materials Chemistry Consortium, which is funded by EPSRC (EP/F067496), for providing computer resources on the UK's national high-performance computing service HECToR and Archer. The authors are grateful to Y. Wimmer, W. Goes, F. Schanovsky and G. Pobegen for valuable and stimulating discussions.

* al-moatasem.el-sayed.10@ucl.ac.uk
† matthew.watkins@ucl.ac.uk
‡ grasser@iue.tuwien.ac.at
§ valeri.afanasiev@fys.kuleuven.be
¶ a.shluger@ucl.ac.uk

[1] H. Li and J. Robertson, J. Appl. Phys. **115**, 203708 (2014).
[2] C. Van de Walle and J. Neugebauer, Nature **423**, 626 (2003).
[3] G. H. Enevoldsen, H. P. Pinto, A. S. Foster, M. C. R. Jensen, W. A. Hofer, B. Hammer, J. V. Lauritsen, and F. Besenbacher, Phys. Rev. Lett. **102** (2009).
[4] K. Kajihara, L. Skuja, M. Hirano, and H. Hosono, Phys. Rev. Lett. **89**, 135507 (2002).
[5] K. Kajihara, L. Skuja, M. Hirano, and H. Hosono, Phys. Rev. B **74**, 094202 (2006).
[6] D. M. Hofmann, A. Hofstaetter, F. Leiter, H. Zhou, F. Henecker, B. K. Meyer, S. B. Orlinskii, J. Schmidt, and P. G. Baranov, Phys. Rev. Lett. **88**, 045504 (2002).
[7] J. Godet and A. Pasquarello, Microelectronic Engineering **80**, 288 (2005).
[8] B. E. Hobbs, "Point defects in minerals," (American Geophysical Union, 1985) pp. 151–169.
[9] D. L. Griscom, Nucl. Instr. Methods B **46**, 12 (1990).
[10] A. G. Revesz, IEEE Trans. Nucl. Sci. **24**, 2102 (1977).
[11] F. B. McLean, IEEE Trans. Nucl. Sci. **27**, 1651 (1980).
[12] D. L. Griscom, J. Appl. Phys. **58**, 2524 (1985).
[13] D. J. DiMaria, E. Cartier, and D. Arnold, J. Appl. Phys. **73**, 3367 (1993).
[14] C. R. Helms and E. H. Poindexter, Rep. Prog. Phys. **57**, 791 (1994).
[15] G. Pobegen, T. Aichinger, and M. Nelhiebel, "Impact of hydrogen on the bias temperature instability," in *Bias Temperature Instability for Devices and Circuits*, edited by T. Grasser (Springer, 2014) pp. 485–506.
[16] L. Skuja, K. Kajihara, M. Hirano, A. Saitoh, and H. Hosono, J. Non-cryst. Sol. **352**, 2297 (2006).
[17] L. Skuja, K. Kajihara, and H. Hirano, M. andHosono, Nucl. Instr. and Meth. in Phys. Res. B **266**, 2971 (2008).
[18] I. A. Shkrob, B. M. Tadjikov, S. D. Chemerisov, and A. D. Trifunac, J. Chem. Phys. **111**, 5124 (1999).
[19] I. A. Shkrob and A. D. Trifunac, J. Chem. Phys. **107**, 2374 (1997).
[20] J. Vitko, J. Appl. Phys. **49**, 5530 (1978).
[21] V. A. Radzig, Kinetika i Kataliz **20**, 456 (1979).
[22] M. Wilde, M. Matsumoto, and K. Fukutani, J. Appl. Phys. **92**, 4320 (2002).
[23] V. V. Afanas'ev, J. M. M. de Nijs, P. Balk, and A. Stesmans, J. Appl. Phys. **78**, 6481 (1995).
[24] A. Stesmans and V. V. Afanas'ev, Appl. Phys. Lett. **72**, 2271 (1998).
[25] V. V. Afanas'ev and A. Stesmans, J. Electrochem. Soc. **148**, G279 (2001).
[26] A. Rivera, A. van Veen, H. Schut, J. M. M. de Nijs, and P. Balk, Solid State Electron. **46**, 1775 (2002).
[27] M. Wilde and K. Fukutani, Surface Sci. Reports **69**, 196 (2014).
[28] R. A. B. Devine, W. L. Warren, J. B. Xu, I. H. Wilson, P. Paillet, and J. L. Leray, J. Appl. Phys. **77**, 1754 (1995).
[29] R. A. B. Devine, D. Mathiot, W. L. Warren, and B. Aspar, J. Appl. Phys. **79**, 2302 (1996).
[30] V. V. Afanas'ev and A. Stesmans, Phys. Rev. B **60**, 5506 (1999).
[31] V. V. Afanas'ev, F. Ciobanu, G. Pensl, and A. Stesmans, Solid State Electron. **46**, 1815 (2002).
[32] V. Afanas'ev and A. Stesmans, Europhys. Lett. **53**, 233 (2001).
[33] V. V. Afanas'ev and A. Stesmans, Phys. Rev. Lett. **78**, 2437 (1997).
[34] A. H. Edwards and G. Germann, Nucl. Instr. and Meth. in Phys. Res. B **32**, 238 (1988).
[35] G. Pacchioni and M. Vitiello, Phys. Rev. B **58**, 7745 (1998).
[36] P. Blöchl, Phys. Rev. B **62**, 6158 (2000).
[37] A. C. T. van Duin, A. Strachan, S. Stewman, Q. Zhang, X. Xu, and W. Goddard, J. Phys. Chem. A **107**, 3803 (2003).
[38] J. C. Fogarty, H. M. Aktulga, A. Y. Grama, A. C. T. van Duin, and S. A. Pandit, J. Chem. Phys. **132**, 174704 (2010).
[39] S. Plimpton, J. Comp. Phys. **117**, 1 (1995).
[40] A.-M. El-Sayed, M. B. Watkins, V. V. Afanas'ev, and A. L. Shluger, Phys. Rev. B **89**, 125201 (2014).
[41] A. Waseda and K. Fujii, IEEE Trans. Instrum. Meas. **56**, 628 (2007).
[42] J. VandeVondele, M. Krack, F. Mohamed, M. Parrinelo, T. Chassaing, and J. Hutter, Comp. Phys. Comm. **167**, 103 (2005).
[43] M. Guidon, J. Hutter, and J. VandeVondele, J. Chem. Theory Comput. **5**, 3013 (2009).
[44] G. Lippert, J. Hutter, and M. Parrinello, Mol. Phys. **92**, 477 (1997).
[45] J. VandeVondele and J. Hutter, J. Chem. Phys. **127**,

114105 (2007).
[46] S. Goedecker, M. Teter, and J. Hutter, Phys. Rev. B **54**, 1703 (1996).
[47] B. Civalleri and P. Ugliengo, J. Phys. Chem. B **104**, 519 (2000).
[48] M. D. Towler, N. L. Allan, N. M. Harrison, V. R. Saunders, W. C. Mackrodt, and E. Apra, Phys. Rev. B **50**, 5041 (1994).
[49] R. Krishnan, J. S. Binkley, R. Seeger, and J. A. Pople, J. Chem. Phys. **72**, 650 (1980).
[50] M. Guidon, J. Hutter, and J. VandeVondele, J. Chem. Theory Comput. **8**, 2348 (2010).
[51] G. Henkelman, B. P. Uberuaga, and H. Jnsson, J. Chem. Phys. **113**, 9901 (2000).
[52] A. Yokozawa and Y. Miyamoto, Phys. Rev. B **55**, 13783 (1997).
[53] P. Bunson, M. D. Ventra, S. Pantelides, R. Schrimpf, and K. Galloway, IEEE Trans.Nucl.Sci. **46**, 1568 (1999).
[54] M. Farnesi Camellone, J. C. Reiner, U. Sennhauser, and L. Schlapbach, Phys. Rev. B **76**, 125205 (2007).
[55] A. H. Edwards, J. A. Pickard, and J. E. Stahlbrush, J. Non-cryst. Solids **179**, 148 (1994).
[56] J. Godet, P. Broqvist, and A. Pasquarello, Appl.Phys.Lett. **91**, 262901 (2007).
[57] J. Godet, F. Giustino, and A. Pasquarello, Phys.Rev.Lett. **99**, 126102 (2007).
[58] A.-M. El-Sayed, Y. Wimmer, W. Goes, T. Grasser, and A. Shluger, To Be Published (2014).
[59] R. Prins, Chem. Rev. **112**, 2714 (2012).
[60] Y. Hwang, R. Engel-Herbert, N. G. Rudawski, and S. Stemmer, J. App. Phys. **108**, 034111 (2010).
[61] C. H. Wang, S. W. Wang, G. Dornboos, G. Astromskas, K. Bhuwalka, R. Cortreras-Guerro, M. Edirisooriya, J. S. Roijas-Ramirez, G. Vellitantis, R. Oxland, M. C. Holland, C. H. Hsieh, P. Ramwall, E. Lind, W. C. Hsu, L.-E. Wernersson, R. Droopad, M. Passlack, and C. H. Diaz, App. Phys. Lett. **103**, 143510 (2013).
[62] J. Swerts, M. Popovici, B. Kaczer, M. Aoulaiche, A. Redolfi, S. Clima, C. Caillat, W. C. Wang, V. V. Afanas'ev, N. Jourdan, C. Olk, H. Hody, S. Van Elshocht, and M. Jurczak, IEEE Electron. Dev. Lett. **35**, 753 (2014).